Frost formation and ice adhesion on superhydrophobic surfaces

Kripa K. Varanasi' , Tao Deng' , J. David Smith, Ming Hsu, and Nitin Bhate

Citation: Appl. Phys. Lett. **97**, 234102 (2010); doi: 10.1063/1.3524513
View online: http://dx.doi.org/10.1063/1.3524513
View Table of Contents: http://aip.scitation.org/toc/apl/97/23
Published by the American Institute of Physics

Frost formation and ice adhesion on superhydrophobic surfaces

Kripa K. Varanasi,[1,a)] Tao Deng,[2,a)] J. David Smith,[1] Ming Hsu,[2] and Nitin Bhate[2]
[1]*Department of Mechanical Engineering, Massachusetts Institute of Technology, Cambridge, Massachusetts 02139, USA*
[2]*Nanotechnology Advanced Technology, GE Global Research Center, Niskayuna, New York 12309, USA*

(Received 25 October 2010; accepted 7 November 2010; published online 7 December 2010)

We study frost formation and its impact on icephobic properties of superhydrophobic surfaces. Using an environmental scanning electron microscope, we show that frost nucleation occurs indiscriminately on superhydrophobic textures without any particular spatial preference. Ice adhesion measurements on superhydrophobic surfaces susceptible to frost formation show increased adhesion over smooth surfaces with a strong linear trend with the total surface area. These studies indicate that frost formation significantly compromises the icephobic properties of superhydrophobic surfaces and poses serious limitations to the use of superhydrophobic surfaces as icephobic surface treatments for both on-ground and in-flight applications. © *2010 American Institute of Physics*. [doi:10.1063/1.3524513]

Ice is a significant problem in various industries including transportation, power, buildings, and agriculture. Ice accumulation can cause hazardous road conditions, down power lines, damage crops, and reduce the performance of and stall aircraft engines, ships, wind turbines, and HVAC systems. Passive deicing systems that prevent ice formation or reduce ice adhesion and accumulation without additional power input or active controls are of particular interest. Hence research on various anti-icing surface treatments including glycol-based deicing sprays and icephobic coatings has been active over several decades.[1–6] Some of these studies indicate that ice adhesion reduces with increasing hydrophobicity of the surface. Recently, the use of hydrophobic surface treatments for reducing ice accretion has been extended to superhydrophobic surfaces.[7–13] Some of these studies show reduced accretion of ice formed from supercooled water that was either sprayed or simply poured onto the test superhydrophobic surfaces.[9–11] Although ice formation from supercooled droplets is important in various practical applications, frost formation is another common mechanism for ice accretion on surfaces. In this paper, we study frost formation and its implications on ice adhesion properties of superhydrophobic surfaces. Based on environmental scanning electron microscope (ESEM) experiments of frost nucleation and growth and macroscopic ice adhesion measurements on superhydrophobic surfaces, we find that icephobic properties of superhydrophobic surfaces can be significantly compromised due to frost formation. These studies provide valuable insights into the design of robust icephobic surfaces.

The nucleation and growth of ice has been an active area of research for several decades.[14–16] According to classical nucleation theory, the free energy barrier ΔG, and the nucleation rate J, for heterogeneous ice nucleation from the vapor phase depends on interfacial energies, lattice mismatch, and radius of curvature.[14] Following Fletcher,[14] we write ΔG and J for a flat noncoherent interface as

$$\Delta G = \frac{\pi \sigma_{\mathrm{IV}} r^{*2}}{3}(2-3m+m^3); \quad J = J_o \exp(-\Delta G/kT), \tag{1}$$

where σ_{IV} is the ice-vapor surface energy and r^* is the critical radius. The parameter m is the ratio of the interfacial energies given by $m=(\sigma_{\mathrm{SV}}-\sigma_{\mathrm{SI}})/\sigma_{\mathrm{IV}}$, where σ_{SV} and σ_{SI} are, respectively, the substrate-vapor and substrate-ice interfacial energies. The critical radius r^* can be related to other thermodynamic quantities as $\ln(p/p_\infty)=2\sigma_{\mathrm{IV}}/n_I kTr^*$, where p is the ambient vapor pressure, p_∞ is the saturated vapor pressure over a flat ice surface at temperature T, n_I is the number of molecules per unit volume of ice, k is the Boltzmann constant, and J_o is a kinetic constant. From Eq. (1), we find that surfaces with spatially uniform intrinsic interfacial energies will be characterized by spatially uniform nucleation energy barrier and rate, thereby resulting in nonpreferential frost nucleation once favorable supersaturation conditions are attained. This effect was apparent in our frost nucleation studies on superhydrophobic surfaces.

We conducted real time frost nucleation and growth studies on superhydrophobic surfaces in an ESEM (FEI Quanta FEG). These surfaces were comprised of an array of hydrophobic silicon posts that were fabricated using a standard photolithography process and coated with a thin hydrophobic layer of (tridecafluoro-1,1,2,2-tetrahydrooctyl) trichlorosilane (Gelest) to impart superhydrophobicity.[17] The ESEM experiments were conducted by cooling the test surface below the freezing point using a cold stage and then increasing the vapor pressure of the chamber until frost nucleation was observed. Snapshot images of the nucleation and growth of frost on these superhydrophobic surfaces taken over a period of 36 s are shown in Fig. 1. These images visibly demonstrate that frost forms indiscriminately all over the superhydrophobic surface texture including post tops, sidewalls, and valleys without any particular spatial preference. The frost layer significantly alters the interfacial properties of the original superhydrophobic surface; the frost-coated hydrophobic posts are hydrophilic and the surface loses its superhydrophobic properties. Apart from the desublimation mechanism described here, another common mechanism for frost formation is condensation followed by freezing.[18] We have reported elsewhere[19] ESEM experiments

[a)]Authors to whom correspondence should be addressed. Electronic address: varanasi@mit.edu. Tel.: 617-324-5608 and dengt@research.ge.com. Tel.: 518-387-5473.

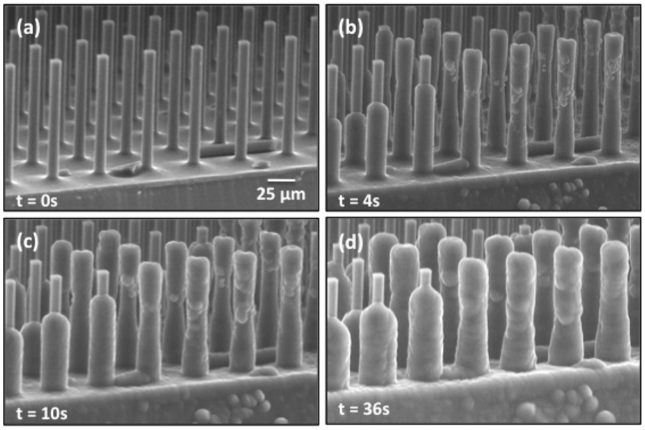

FIG. 1. ESEM images of frost formation on a superhydrophobic surface comprising of an array of hydrophobic square posts with width, edge-to-edge spacing, and aspect ratio of 15 μm, 30 μm, and 7, respectively. (a) Dry surface. [(b)–(d)] Snapshot images of frost formation on the surface. The intrinsic water contact angle of the hydrophobic coating on the posts is ~110°. The surface is maintained at a temperature −13 °C by means of a cold stage accessory of the ESEM. At the beginning of the experiment the chamber pressure is maintained at ~100 Pa, well below the saturation pressure to ensure a dry surface. The vapor pressure in the chamber is then slowly increased until frost nucleation is observed. Frost nucleation and growth occurs without any particular spatial preference on all of the available area including post tops, sidewalls, and valleys due to the uniform intrinsic wettability of the surface.

of condensation on superhydrophobic surfaces that show similar nonpreferential nucleation of water leading to the loss of superhydrophobicity. These nucleation studies can explain the recent observations of lowering of water contact angles on superhydrophobic surfaces near the freezing point.[20] Hence, either via desublimation or condensation, once appropriate supersaturation conditions are achieved, indiscriminate frost formation is unavoidable on surfaces with spatially uniform intrinsic surface energy resulting in the loss of superhydrophobicity, increased wetting, and complete infiltration of the surface textures by frost. This leads to increased ice-surface contact area, increased ice adhesion, and ultimately loss of icephobic properties of the original superhydrophobic surface.

To verify the above hypothesis, systematic droplet impact experiments and ice adhesion measurements were carried out on various superhydrophobic surfaces. Droplet impact experiments were conducted on superhydrophobic surfaces exposed to ambient air with a relative humidity of 70% at two conditions: ambient temperature 18 °C (dry surface) and at −5 °C (cold surface) using a Peltier plate. For cold surfaces, the sample was purged with nitrogen to prevent condensation or desublimation as the Peltier plate was being cooled. Once the sample was cooled to −5 °C, nitrogen flow was stopped and frost was allowed to form on the sample for 10 min before conducting droplet impact experiments. As shown in Fig. 2(c) for a representative superhydrophobic surface, frost readily forms on the cold surface and significantly alters the wetting behavior of the surface—droplets that typically recoil from the dry surface under ambient conditions as shown in Fig. 2(b) are seen to undergo Cassie-to-Wenzel transition[21] and remain pinned on the frosted surface as shown in Fig. 2(c). Frost formation can therefore result in the loss of superhydrophobic properties of the surface.

The ice adhesion strength was measured using an apparatus consisting of a load cell (Imada Z2-44), Peltier cooling stage (TECA), and water-filled cuvettes that were frozen onto the test surfaces as shown in Fig. S1.[17] The load cell tip was driven parallel to the ice-surface interface into the ice columns at 5 mm/s and the peak force required to fracture the ice-surface interface as well as the fracture mode (cohesive or adhesive) was recorded. The peak force was divided by the ice cross-sectional area to obtain an average adhesion strength of the ice-surface interface. The details of the test apparatus and test procedure are provided in the supplementary material.[17] Ice adhesion measurements were first performed on smooth surfaces to establish a benchmark. Materials tested range from hydrophilic to hydrophobic[17] and the resulting ice adhesion strengths of the various smooth surfaces plotted in Fig. S2 as a function of the water contact angle show a clear trend in the decreasing ice adhesion strength as the surface becomes more hydrophobic in agreement with literature.[3–6] Moreover, the fracture of the ice-surface interface was observed to be cohesive for the hydrophilic samples and adhesive for the hydrophobic samples consistent with the adhesion measurements.

Next, we conducted systematic ice adhesion measurements on a series of superhydrophobic surfaces comprising polydimethysiloxane (PDMS) post arrays replicated from silicon masters. We utilize PDMS because silicon posts are brittle and break easily during ice adhesion measurements. Representative optical images shown in Figs. 3(a)–3(d) illustrate the excellent quality of replication. The texture parameters such as post width a, spacing-to-width ratio b/a, and aspect ratio h/a were systematically varied. Arrays consist of periodic posts that are 10 μm in height, 5–15 μm in width, and 5–45 μm in spacing. Wetting measurements indicate that droplets on the PDMS post surfaces are in a Cassie state and water contact angles range from 145° to 163°, all values

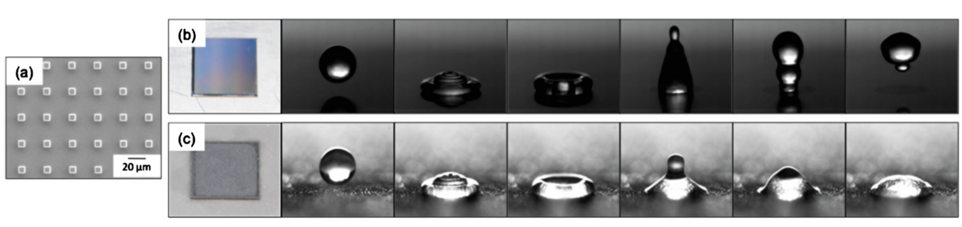

FIG. 2. (Color online) Droplet impact measurements on dry and frosted superhydrophobic surface conducted using droplets of 1 mm radius impacting the surface at velocity ~0.7 m/s. (a) Top view SEM image of the representative Si post array surface with width, edge-to-edge spacing, and aspect ratio of 10 μm, 20 μm, and 1, respectively. (b) Photograph of the dry surface along with sequential high-speed video images of droplet impact. As expected, droplet recoils from the surface, as the antiwetting capillary pressure is greater than the dynamic wetting pressures (see Ref. 25). (c) Photograph of the frosted surface along with sequential high-speed video images of droplet impact. Frost alters the wetting properties of the surface, making the surface hydrophilic, causing Cassie-to-Wenzel wetting transition of the impacting drop, subsequent pinning and formation of "Wenzel" ice on the surface.

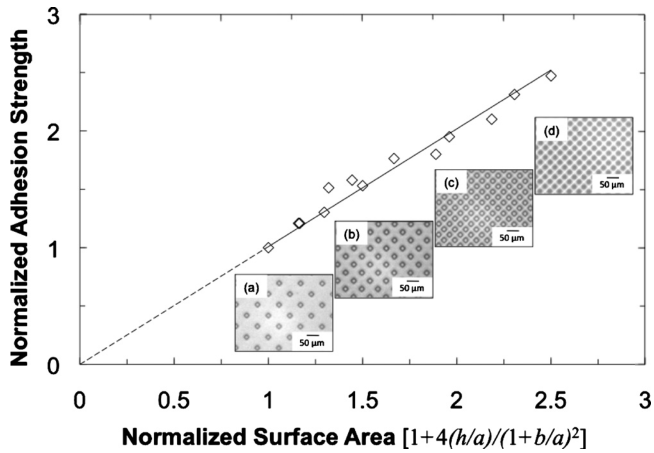

FIG. 3. Plot of the measured ice adhesion strength of the textured surfaces normalized by the measured ice adhesion strength of the smooth surface as a function of total surface area normalized by the projected area. The ice adhesion measurements on textured and smooth PDMS surfaces were conducted at −15 °C using the apparatus described in supplementary material (Ref. 17). The normalized ice adhesion strength increases with normalized surface area and shows a strong linear trend. The best linear fit to the data (solid line, correlation coefficient $R^2=0.96$) has a slope of one and passes through the origin (extrapolated using a dashed line) indicating that ice is contacting all available surface area. Insets [(a)–(d)] are top view optical images of representative replicated PDMS post arrays from sparse to dense spacing ($a=15$ μm, $h=10$ μm, $b=45$, 30, 15, and 5 μm, respectively) showing the excellent quality of replication.

that are well beyond the water contact angle of the smooth PDMS surface of ~115°. However, ice adhesion strength of these textured surfaces was found to be larger than that of the smooth surface of the same material. In fact, plotting the ice adhesion strength of the textured surfaces normalized by the ice adhesion strength of the flat surface as a function of total surface area normalized by the projected area $1+4(h/a)/(1+b/a)^2$ reveals a strong linear trend (with correlation coefficient $R^2=0.96$) with a slope of one as shown in Fig. 3, indicating that ice is contacting all available area of the textured surface. During the freezing process the post arrays are exposed to water vapor that is in thermodynamic equilibrium with the column of water supported by the posts inside the water-filled cuvettes. As the post array is cooled below the freezing point of water, frost forms indiscriminately on all available surfaces (similar to ESEM images of Fig. 1), making the surfaces more hydrophilic and enabling the liquid water to then wet and form "Wenzel" ice. Thus, it is not surprising that we observe adhesive contact between ice and all available surfaces on the superhydrophobic textures, which validates our hypothesis of increased adhesion due to frost formation. Therefore, ice adhesion will be enhanced by superhydrophobic textures whenever frost can form indiscriminately on the surface. The best linear fit to the adhesion measurements of Fig. 3 passes through the origin (extrapolated using a dashed line), suggesting that ice adhesion strength can be lowered below that of a smooth surface by reducing the ice-surface contact area. Hence approaches that can spatially control nucleation[19,22] (e.g., promote nucleation on top portions of the texture[19] to form "Cassie" ice) could reduce ice adhesion and improve the robustness of textured surfaces for icephobicity.

In summary, we show that frost formation could significantly compromise the icephobic properties of superhydrophobic surfaces. ESEM visualization clearly shows that frost nucleation occurs on all areas of the superhydrophobic surface, including post tops, sidewalls, and valleys of the surface texture without any particular preference, leading to the loss of superhydrophobic properties. Ice adhesion measurements on superhydrophobic surfaces susceptible to frost formation indicate increased adhesion over smooth surfaces with a strong linear trend with the total surface area. Frost formation on structures such as wind turbines, oil platforms, communication towers, HVAC equipment, etc., in cold regions is a common occurrence. In-flight ice accretion on aircraft surfaces is usually attributed to the freezing of supercooled water droplets suspended in clouds that come into contact with aircraft surfaces. However, recent studies show that icing clouds could be unexpectedly supersaturated resulting in heterogeneous ice nucleation.[23,24] Hence, frost formation could also be an important in-flight ice accretion mechanism on aircraft surfaces. Therefore, it is important to consider frost formation while designing icephobic surfaces and extreme caution must be exercised in the use of superhydrophobic surfaces for icephobic surface treatments in both on-ground and in-flight applications.

We thank Dr. Margaret Blohm and Nanotechnology Advanced Technology Program of GE Global Research for support. K.K.V. acknowledges the support from d'Arbeloff Career Development Chair and Reed Award at MIT.

[1]H. H. G. Jellinek, J. Colloid Sci. **14**, 268 (1959).
[2]M. Landy and A. Freiberger, J. Colloid Interface Sci. **25**, 231 (1967).
[3]V. K. Croutch and R. A. Hartley, J. Coat. Technol. **64**, 41 (1992).
[4]V. F. Petrenko and R. W. Whitworth, *Physics of Ice* (Oxford University Press, New York, 1999).
[5]V. F. Petrenko and S. Peng, Can. J. Phys. **81**, 387 (2003).
[6]A. J. Meuler, J. D. Smith, K. K. Varanasi, J. Mabry, G. H. McKinley, and R. E. Cohen, ACS Appl. Mater. Interfaces **2**, 3100 (2010).
[7]H. Saito, K. Takai, and G. Yamauchi, Mater. Sci. Res. Int. **3**, 185 (1997).
[8]T. Kako, A. Nakajima, H. Irie, Z. Kato, K. Uematsu, T. Watanabe, and K. Hashimoto, J. Mater. Sci. **39**, 547 (2004).
[9]N. Bhate, M. Hsu, G. O'Neil, T. Deng, S. Okuyama, J. Stein, N. Turnquist, and K. K. Varanasi, US 11/487023, EP 1750018, 2005.
[10]S. A. Kulinich and M. Farzaneh, Langmuir **25**, 8854 (2009); Appl. Surf. Sci. **255**, 8153 (2009).
[11]L. Cao, A. K. Jones, V. K. Sikka, J. Wu, and D. Gao, Langmuir **25**, 12444 (2009).
[12]P. Tourkine, M. Le Maerrer, and D. Quere, Langmuir **25**, 7214 (2009).
[13]L. Mischenko, B. Hatton, V. Bahadur, J. A. Taylor, T. Krupenkin, and J. Aizenberg, ACS Nano (2010).
[14]N. H. Fletcher, *The Physics of Rainclouds* (Cambridge University Press, Cambridge, 1966); J. Chem. Phys. **29**, 572 (1958).
[15]K. G. Libbrecht, Rep. Prog. Phys. **68**, 855 (2005).
[16]C. A. Stan, G. F. Schneider, S. S. Shevkoplyas, M. Hashimoto, M. Ibanescu, B. J. Wiley, and G. M. Whitesides, Lab Chip **9**, 2293 (2009).
[17]See supplementary material at http://dx.doi.org/10.1063/1.3524513.
[18]B. Na and R. L. Webb, Int. J. Heat Mass Transfer **46**, 3797 (2003).
[19]K. K. Varanasi, M. Hsu, N. Bhate, W. Yang, and T. Deng, Appl. Phys. Lett. **95**, 094101 (2009).
[20]R. Karmouch and G. G. Ross, J. Phys. Chem. C **114**, 4063 (2010).
[21]N. A. Patankar, Langmuir **26**, 8941 (2010).
[22]J. Aizenberg, A. J. Black, and G. M. Whitesides, Nature (London) **398**, 495 (1999).
[23]T. Peter, C. Marcolli, P. Spichtinger, T. Corti, M. B. Baker, and T. Koop, Science **314**, 1399 (2006).
[24]B. J. Murray, T. W. Wilson, S. Dobbie, Z. Cui, S. Al-Jumur, O. Mohler, M. Schnaiter, R. Wagner, S. Benz, M. Niemand, H. Saathoff, V. Ebert, S. Wagner, and B. Karcher, Nat. Geosci. **3**, 233 (2010).
[25]T. Deng, K. K. Varanasi, M. Hsu, N. Bhate, C. Keimel, J. Stein, and M. Blohm, Appl. Phys. Lett. **94**, 133109 (2009).